Chapter 2
Theory of the Piezoresistive Effect in p-Type 3C-SiC

This chapter qualitatively explains the piezoresistive effect in p-type 3C-SiC based on the hole transfer mechanism and the conduction effective mass change due to the deformation of energy band under strain. To explain this phenomenon, the ideas of energy band structure and band deformation of 3C-SiC are discussed. Furthermore, the description of piezoresistive coefficients are also presented in the rest of this chapter.

2.1 Energy Band of 3C-SiC

2.1.1 Crystallographic and Energy Band Structure of 3C-SiC

The basic unit of 3C-SiC is based on the covalent bond between Si and C atoms, forming tetrahedrons. As such each Si atom bonds with other four C atoms to form SiC_4, while each C atom bonds with other four Si atoms to form C_4Si [1]. Different staking orders of these tetrahedrons result in different poly types of SiC, where the stacking sequence of these poly types can be presented using the 'ABC' notation, in which A, B and C represent the three sites available in one sub-lattice. For instance, the stacking sequence of a unit of 3C-SiC is ABC, while those of 4H-SiC and 6H-SiC are ABCB, and ABCACB, respectively [2]. Cubic SiC has been named as 3C-SiC, since each unit of its stacking order consists of three Si-C bi-layers, while the letter 'C' indicates that the symmetry of this poly type is cubic. The same rule has also been applied for other poly types such as 4 H and 6H-SiC in which numbers 4 and 6 indicate the number of Si-C bi-layers within one staking unit, and the letter 'H' stands for their hexagonal symmetry. Figure 2.1 shows a unit of SiC stacking tetrahedron and the stacking sequence (ABC) of 3C-SiC.

H.-P. Phan, *Piezoresistive Effect of p-Type Single Crystalline 3C-SiC*,
Springer Theses, DOI 10.1007/978-3-319-55544-7_2

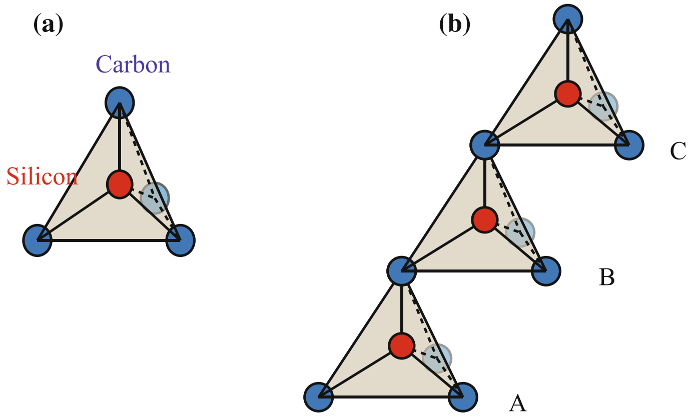

Fig. 2.1 **a** a unit of SiC_4 tetrahedron; **b** Stacking order of 3C-SiC

Figure 2.2a show the face centered crystal of 3C-SiC with its lattice constant of 4.36 Å [3]. Since semiconductor devices are built on or near the surface of semiconductor, the information of surface orientation are important. To define the orientation of a semiconductor plane, Miller indices are widely used [4]. The Miller indices of the most common planes in 3C-SiC are shown in Fig. 2.2b–d, including (100), (110), and (111) planes.

The band structure of a semiconductor is represented using the $E - k$ (Energy-momentum) diagram, where k is the momentum vector in the reciprocal space. The reciprocal lattice can be obtained from the real crystal lattice using a Fourier transformation and the band structure of a crystalline can be obtained by solving the Schrödinger equation of an one-electron problem [5]:

$$\left[-\frac{\hbar^2}{2m^*}\nabla^2 + V(r)\right]\Psi(r,k) = E(k)\Psi(r,k) \tag{2.1}$$

where $\hbar = h/2\pi$ (i.e. $h = 6.626 \times 10^{-34}$ m^2kg/s is Plank's constant), m^* is the effective mass of electron, $V(r)$ is a potential energy in the direct lattice space, and $\Psi(r,k)$ is the wave function. Since the potential energy $V(r)$ is a periodic function, the energy $E(k)$ can be completely characterized in a single primitive cell in the reciprocal space. This primitive cell is defined as the first Brillouin zone (also known as the Brillouin zone), which can be constructed by drawing perpendicular bisector planes in the reciprocal lattice from the chosen center to the nearest equivalent reciprocal lattice sites. A detailed explanation of the reciprocal transformation and the construction of the Brillouin zone can be found in the book of S.M. Sze and Kwok K. Ng [4].

Figure 2.3 shows the first BZ of the face centered semiconductors, including Si and 3C-SiC. In this figure, the Γ point is the center of the BZ, the X point is the center of the square surfaces, and the L point is the center of the hexagonal surfaces,

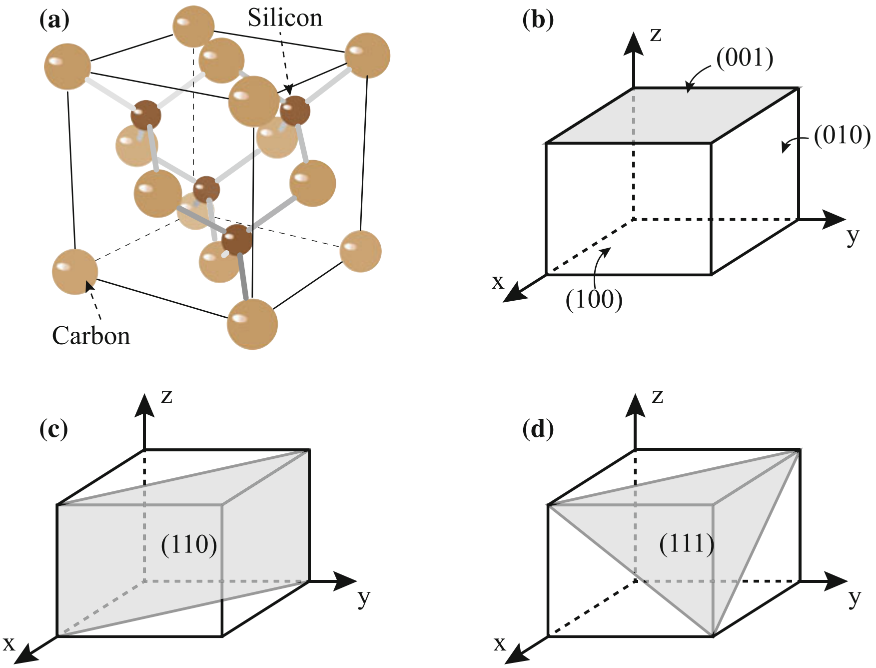

Fig. 2.2 **a** Crystal structure of 3C-SiC; **b**, **c**, **d** Common crystal planes of 3C-SiC

Fig. 2.3 The first Brillouin Zone (BZ) of face centered crystal

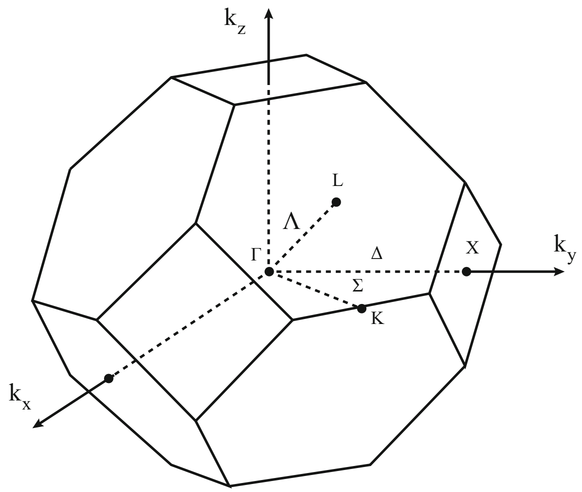

respectively. Additionally, Δ is the vector connecting the Γ point and the *X* point, while Λ is the vector connecting the Γ point and the *L* point.

The energy band of 3C-SiC was described in the paper of Hemstreet et al., calculated based on a non-local version of the empirical-pseudopotential method

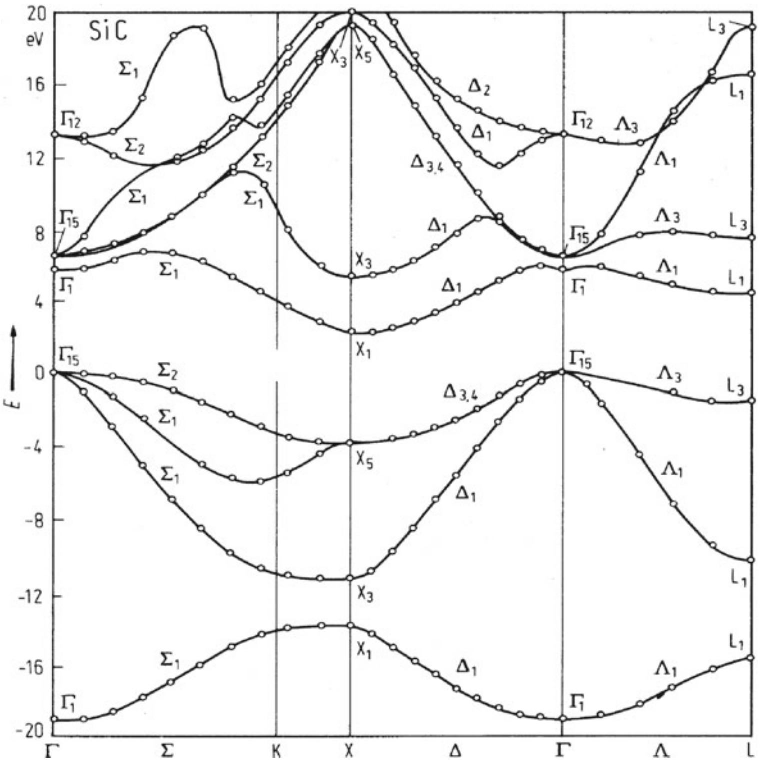

Fig. 2.4 The energy band structure of 3C-SiC in k-space. Reprint with permission from [6]

[6]. Accordingly, 3C-SiC is an indirect semiconductor, having its lowest conduction bands located at the X point, and its highest valance bands located at Γ point, as shown in Fig. 2.4. The indirect energy gap between X point and Γ point was calculated to be 2.33 eV, which is in consistent agreement with experimental results.

Since carriers (electrons in the conduction bands and holes in the valence bands) fill the lower energy bands first, the conductivity of 3C-SiC (σ_c) depends on the carrier concentration and mobility of the electrons in the bottom conduction band and the holes in the top valence band, which is defined in the following equation:

$$\sigma_c = q(\mu_e N_e + \mu_h N_h) \tag{2.2}$$

where q is the unit charge (i.e. 1.6021765×10^{19} C), μ_e and μ_h are the mobility of electron and hole, and N_e and N_h are the concentration of electrons and holes, respectively. In case of p-type 3C-SiC, holes are the major carriers, therefore its electrical conductivity is dominated by the hole mobility and concentration.

$$\sigma_c = q\mu_h N_h \tag{2.3}$$

where, the hole concentration (N_h) follows Boltzmann distribution:

$$N_h = N_V F_{1/2}\left(-\frac{E_F - E_V}{k_B T}\right) \tag{2.4}$$

where, N_V is the effective density of state, $F_{1/2}$ is the Fermi-Dirac integral, $E_F - E_V$ is the difference energy between the Fermi level and top valence bands, k_B is the Boltzmann's constant (i.e. 1.38×10^{-23} m^2.kg.s^{-2}.K^{-1}), and T is the absolute temperature, respectively. Furthermore, the mobility of hole is defined as:

$$\mu_h = \frac{q}{m_h^*}\tau_h \tag{2.5}$$

here m_h^* and τ_h are the hole effective mass and mean free path (i.e. the average time between two successive collisions of a particle to the lattice) of hole. Additionally, the effective mass can be expressed as a function of a wave-vector space:

$$m_h^* = \frac{h}{4\pi^2}\left(\frac{d^2E}{dk^2}\right)^{-1} \tag{2.6}$$

Equation 2.6 indicates that, in the $E - k$ diagram, a large energy curvature (parabolic approximation) results in a smaller hole effective mass. Therefore, in p-type 3C-SiC, the top two valance bands were named based on this properties, in which, the light hole has a smaller effective mass than heavy hole due to its larger energy curvature. Furthermore, substitute Eq. 2.5 into Eq. 2.3, the conductivity is:

$$\sigma_c = \frac{q^2 N_h \tau_h}{m_h^*} \tag{2.7}$$

Evidently, from Eqs. 2.4, 2.6, and 2.7, any change in band energy will result in a change of hole concentration (N_h) as well as hole effective mass (m_h^*), consequently changing the conductivity of p-type semiconductors. The change of these parameters under strain is presented in the following sections.

2.1.2 *Principle of the Piezoresistive Effect in p-Type 3C-SiC*

The piezoresistive effect in p-type semiconductor has been extensively investigated since the pioneering work of Smith in 1954 [7]. Its physical origin is considered to be the hole transfer and conduction mass shift mechanisms following the deformation of the top valence bands under strain. To understand the deformation of the top valence band, a simple model of one dimensional (1-D) lattice is introduced. Figure 2.5 shows the 1-D lattice model in which a non-interacting electron moves in a periodic 1-D array of potential wells created by positive ions arranged in a periodic order.

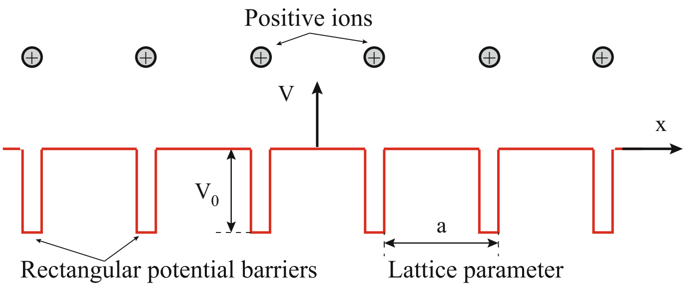

Fig. 2.5 Schematic sketch of 1-D lattice with approximated rectangular potentials

According to the approximation of Kronig and Penney, the potentials caused by the interaction between ions can be simplified as rectangular potential barriers spaced by the lattice parameter [8]. The solution of the Schrödinger's equation in this case is as follows [9]:

$$\cos(ka) = \cos(\alpha a) + \frac{m}{\hbar^2 \alpha} \sin(\alpha a) \tag{2.8}$$

where a is the lattice parameter, m is the free electron mass, and α is given by: $\alpha^2 = 2mE/\hbar^2$. Thus, at each wave vector k, the allowed energies (E) of the electron in the 1-D lattice are the solutions of Eq. 2.8.

Based on these solutions of E, the allowed energy bands of a non interacting electron in the 1-D lattice are plotted in Fig. 2.6 (the black solid curves) [9]. Additionally, from Eq. 2.8, by applying a mechanical strain to the 1-D lattices, the lattice size will be modified from a_0 to $(a_0 + \varepsilon a_0)$, resulting in a different solution of energy E at

Fig. 2.6 Energy band modification under mechanical strains in the 1-D lattice model [9]

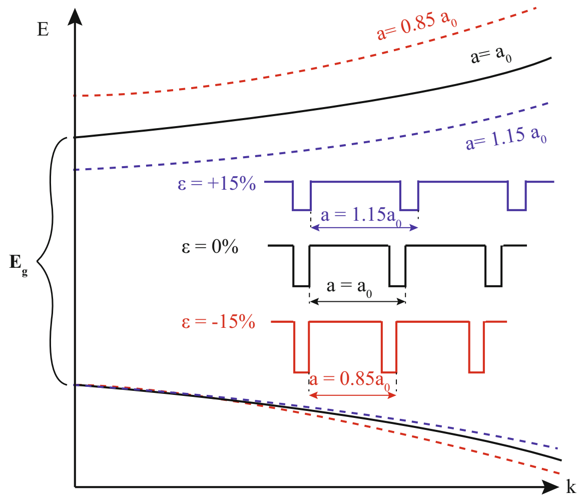

the wave vector k. As such, the simulation results reported by Rowe indicated that, applying strain of $\pm 15\%$ will cause the energy level (E) to shift up and down, leading to a change in the band gap between the allowed energy bands, as shown in the red and blue dashed lines of Fig. 2.6. These results indicate that the energy band structure of 1-D lattice can be modified by applying external mechanical strains.

For 3-D lattice crystals, the model is more complicated, and more complex calculation/simulation are required to estimate the stress dependence of the energy band structure. However, the principle is the same as the simple case of the 1-D lattice. Utilizing the theory of energy band modification under strain, the piezoresistive effect in semiconductors have been theoretically explained. Among various cubic crystalline semiconductors, the theory of the piezoresistive effect in Si has been extensively studied, and the theory of the strain effect on electrical conductivity in other materials has been developed by extending the model of Si. The next section will discuss the theory of the piezoresistance of p-type Si, based on that a qualitatively explanation of that phenomenon in p-type 3C-SiC is presented.

In the energy band structure of Si, two bands locate at the top valence, which are heavy hole and light hole bands. The spin-orbit split-off band locates far from the former bands (0.044 eV), therefore it can be negligible in the consideration of the electrical conduction in p-type Si. The band energies of heavy hole and light hole in Si are given in the following equation, using a parabolic approximation in which the electron effective mass is considered to be constant at the region near to the band extrema in the $E-k$ diagram [10]:

$$E(k) = E_{V0} + \frac{\hbar^2}{2m_0}\left\{Ak^2 \pm \sqrt{B^2k^4 + C^2(k_x^2k_y^2 + k_y^2k_z^2 + k_z^2k_x^2)}\right\} \tag{2.9}$$

where the $+$ sign corresponds to the light hole, while the $-$ sign corresponds to the heavy hole, E_{V0} is the top energy level in valence bands, and A, B, and C are inverse mass parameters, respectively. Under a mechanical strain, the lattice constants of Si and the symmetry of Si crystal will change. As such, a hydrostatic-compressive pressure will reduce its lattice size, while a tensile stress in [110] orientation will reshape Si crystal from a cubic to an orthorhombic structure. Since the lattice size and the symmetry of Si are changed under a mechanical strain/stress, its energy band is expected to be deformed, which also occurs in the 1-D lattice as discussed above. The deformation of the heavy and light holes was driven by Bir and Pikus [11], using the following equation:

$$E(\varepsilon, k) = E(0, k) \pm \frac{E_{\varepsilon k}}{2\sqrt{E_k}} \pm \frac{1}{\Lambda}E_{\varepsilon k} \tag{2.10}$$

where $E(0, k)$ is the strain-free energy of heavy hole and light hole presented in Eq. 2.9, while $E_{\varepsilon k}$ is an energy function of applied strain (ε) and wave vector (k), which is related to the strain tensor through a set of potential deformations (b and d) [12]:

$$E_{\varepsilon k} = Bb[3(k_x^2\varepsilon_{xx} + k_y^2\varepsilon_{yy} + k_z^2\varepsilon_{zz}) - k^2\varepsilon] + 3Dd(k_xk_y\varepsilon_{xy} + k_yk_z\varepsilon_{yz} + k_zk_x\varepsilon_{zx}) \tag{2.11}$$

here ε_{ij} are the six elements of the strain tensor in a 3-D coordinate. Consequently, the hole energy shift and the hole conduction mass shift under strain can be obtained as follows. The energy shift in heavy hole and light hole is:

$$\Delta E_{\varepsilon,k} = \pm\frac{E_{\varepsilon k}}{2\sqrt{E_k}} \tag{2.12}$$

and the conduction mass shift in these band is:

$$\Delta\frac{1}{m} = \pm\frac{1}{\Lambda}E_{\varepsilon k} \tag{2.13}$$

where the + sign corresponds to the heavy hole, and − sign corresponds to the light hole.

Figure 2.7 shows a schematic sketch of the splitting in heavy hole and light hole and the deformation of their energy surfaces under strain. Accordingly, given that a uniaxial strain is applied in [111] orientation of p-type Si, the heavy holes will shift up while the light hole will shift down. The energy surfaces of these bands are also warped due to the degeneracy. As such, the energy surfaces are elongated and become oblate ellipsoids, having axial symmetry along the direction of the applied strain [13].

Next, the electrical conductivity (or resistivity) of p-type Si under strain is considered. Neglecting the influence of spin-orbit split-off band, the conductivity of p-type Si is approximated as:

$$\sigma_{Si} = q^2\tau_h(p_{hh}/m_{hh} + p_{lh}/m_{lh}) \tag{2.14}$$

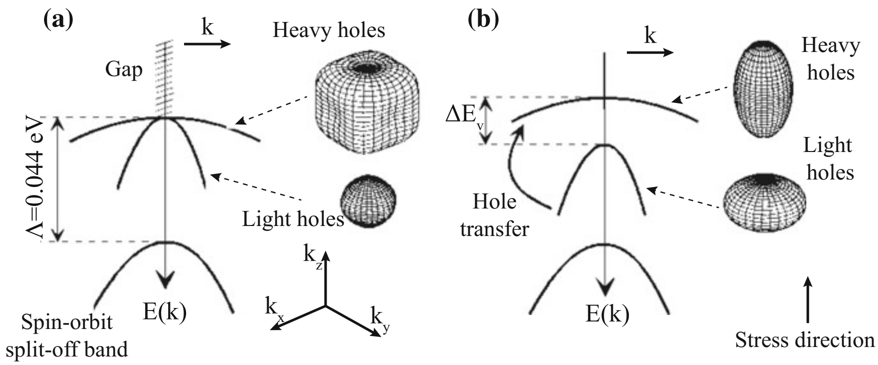

Fig. 2.7 Strain effect on the top valence band of p-type Si. Reprint with permission from [13]

where p and m are hole concentration and effective mass, while the subscription hh and lh indicate heavy hole and light hole.

Note that, since the concentration of hole follows the Boltzmann distribution, as presented in Eq. 2.4, the splitting and warping of heavy hole and light hole cause a change in the hole concentration in these two bands, following the rule that hole will move from higher energy levels to lower energy levels. This change in hole concentration can be quantified as:

$$\Delta P_{\mathrm{i}} = -\frac{N_{\mathrm{V,i}}\Delta(E_{\mathrm{V,i}} - E_{\mathrm{F}})}{k_{\mathrm{B}}T}F_{-1/2}(\eta_{\mathrm{F}}) \tag{2.15}$$

where $\eta_{\mathrm{F}} = -(E_{\mathrm{F}} - E_{\mathrm{V,i}})/(k_{\mathrm{B}}T)$ is the reduced Fermi energy [4], and $\Delta(E_{\mathrm{V,i}} - E_{\mathrm{F}})$ is the energy shift with respect to the Fermi level (E_{F}). Additionally, assume that the total number of holes remains constant, and hole transfer only occurs at the top valence bands (e.g. between heavy hole and light hole), hence:

$$\Delta P_{\mathrm{hh}} + \Delta P_{\mathrm{lh}} = 0 \tag{2.16}$$

Therefore, from Eqs. 2.15 and 2.16, the shift of the Fermi level is [12]:

$$\Delta E_{\mathrm{F}} = \frac{\sum_{i=1}^{2}\Delta E_{\mathrm{V,i}}N_{\mathrm{V,i}}}{\sum_{i=1}^{2}N_{\mathrm{V,i}}}F_{-1/2}(\eta_{\mathrm{F}}) \tag{2.17}$$

Consequently, the change in the concentration of heavy hole and light hole due to the shift of energy bands can be driven using the following equation:

$$\Delta P_{\mathrm{i}} = \frac{\Delta E_{\mathrm{V,i}}\sum_{i=1}^{2}N_{\mathrm{V,i}} - \sum_{i=1}^{2}(\Delta E_{\mathrm{V,i}}N_{\mathrm{V,i}})}{k_{\mathrm{B}}T\sum_{i=1}^{2}N_{\mathrm{V,i}}}F_{-1/2}(\eta_{\mathrm{F}}) \tag{2.18}$$

Based on Eqs. 2.13 and 2.18, the change of the conductivity in p-type Si is given by [14]:

$$\Delta\sigma_{\mathrm{Si},\varepsilon} = q^2\tau[\Delta p_{\mathrm{i}}\frac{1}{m_{\mathrm{i}}} + p_{\mathrm{i}}\Delta(\frac{1}{m_{\mathrm{i}}})] \tag{2.19}$$

Equation 2.19 indicates that both hole transfer (ΔP_{i}) and conduction mass shift ($\Delta(\frac{1}{m_{\mathrm{i}}})$) play an important role in the change of the electrical conductivity in p-type Si. Furthermore, experimental results and theoretical calculations reported in the literature also showed that the relative conductivity change of p-type Si per unit strain was approximately 100 which is two orders of magnitude larger than the change due to geometry. This indicated that the deformation of energy band structure in Si, resulting in the re-population of charge carrier and charge conduction mass, is the physical origin of the piezoresistive effect of p-type Si. Extending this established theory in Si, the piezoresistive effect of p-type 3C-SiC can be qualitatively presented as follows.

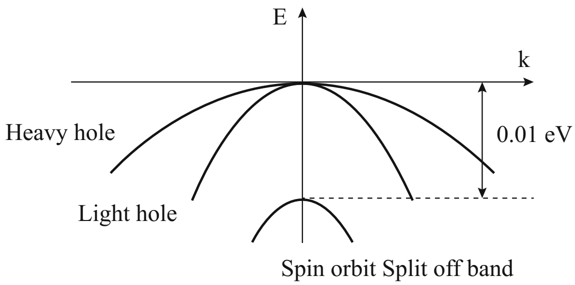

Fig. 2.8 Schematic sketch of the top valence band in p-type 3C-SiC

Because the top valence band of 3C-SiC also consists of three bands, similar to the case of Si, the piezoresistive effect in p-type 3C-SiC can be qualitatively explained using the model of Si. The difference between 3C-SiC and Si is that in 3C-SiC, the distance between the spin-orbit split-off band and the heavy/light holes is only 0.01 eV as shown in Fig. 2.8, the influence of this band should be taken into account [15]. This assumption was also made for the case of p-type diamond crystal, where the distance between spin-orbit split off band to the other two bands is also relatively small [16, 17].The conductivity of p-type 3C-SiC is given by [16]:

$$\sigma_{\mathrm{SiC}} = q^2\tau(P_{\mathrm{SiC,hh}}/m_{\mathrm{SiC,hh}} + P_{\mathrm{SiC,lh}}/m_{\mathrm{SiC,lh}} + P_{\mathrm{SiC,ss}}/m_{\mathrm{SiC,ss}}) \tag{2.20}$$

here the subscriptions hh, lh, and ss stand for heavy hole, light hole and spin-orbit split-off bands, respectively. Since the distribution of holes at the top valence bands and hole conduction mass depend on their energy levels as well as the interaction between the heavy hole, light hole, and and the spin-orbit split-off bands, any change in band energy structure induced by a mechanical strain could cause a change in the conductivity of p-type 3C-SiC (σ_{SiC}).

Numerous studies regarding the strain effect on energy band structure of 3C-SiC have been reported in the literature. Lu et al. used the linear muffin-tin orbitals (LMTO) method and the atomic-sphere approximation to investigate the influence of mechanical strain on the band structure of 3C-SiC [18]. The theoretical results showed that under a biaxial strain in (100) plane, energy band splitting could occur at L, X and Γ points. From the simulation results calculated based on the LMTO method, the energy splitting due to a biaxial strain at the Γ point (Δ_Γ) is approximated by the following equation:

$$\Delta E_\Gamma = b|\varepsilon_{\mathrm{xx}} - \varepsilon_{\mathrm{zz}}| + c(\varepsilon_{\mathrm{xx}} - \varepsilon_{\mathrm{zz}})^2 \tag{2.21}$$

where b and c are deformation potentials. In addition, the simulation results also showed that under a large bi-axial strain of above 8%, the direct gap at Γ point ($\Gamma_{15\mathrm{v}} - \Gamma_{1\mathrm{v}}$) will rapidly decrease in comparison to the indirect gap ($\Gamma_{15\mathrm{v}} - X_{1\mathrm{c}}$), turning 3C-SiC from an indirect material to a direct semiconductor. The authors, therefore, suggested that this interesting phenomenon could be of interest for the development of strain sensors and optical sensors. Rahimi et al. reported the bi-axial tensile stress on Al/p-type 3C-SiC/Al back to back Schottky diode [19]. Accordingly, applying a bi-axial stress in 3C-SiC will cause heavy hole and light hole in the valance band to split, where the heavy hole will be located higher in respect to the light hole. The split of these bands results in the change of band gap in 3C-SiC, thus changing the barrier of the Schottky diode. The change of this barrier can modify the current density of Al/SiC heterojunction.

The above-mentioned theoretical studies indicated that applying a mechanical strain could deform and shift the top valence bands in p-type 3C-SiC [18, 19]. As a result, this band deformation and shifting will change the hole concentration following the Boltzmann distribution (i.e. $P_{\mathrm{SiC,i}}$ becomes $P_{\mathrm{SiC,i}} + \Delta P_{\mathrm{SiC,i}}$), which is much the same as the case of Si described in the previous section. Additionally, the split of the top valance bands will result in the change in the interaction between heavy hole, light hole, and the spin-orbit split-off band, which causes the effective mass in these bands to be changed (i.e. $\frac{1}{m_{\mathrm{SiC,i}}}$ becomes $\frac{1}{m_{\mathrm{SiC,i}}} + \Delta\frac{1}{m_{\mathrm{SiC,i}}}$). Therefore, applying a strain is expected to significantly change the electrical conductivity of p-type 3C-SiC:

$$\frac{\Delta\sigma_{\mathrm{SiC},\varepsilon}}{\sigma_{\mathrm{SiC}}} = \frac{\sum_{i=1}^{3}\left(\Delta p_{\mathrm{SiC,i}}\frac{1}{m_{\mathrm{SiC,i}}} + p_{\mathrm{SiC,i}}\Delta\left(\frac{1}{m_{\mathrm{SiC,i}}}\right)\right)}{\sum_{i=1}^{3} p_{\mathrm{SiC,i}}\frac{1}{m_{\mathrm{SiC,i}}}} \tag{2.22}$$

where the subscription $i = 1, 2, 3$, stands for the heavy hole, light hole, and spin-orbit split-off bands, respectively. Due to the complexity of the valance band (the warping of heavy hole and light hole, as well as the strong interaction between these bands with the spin-orbit split off band), to date these has been no quantitative estimation/calculation of the piezoresistive effect in p-type 3C-SiC. Therefore, more theoretical studies need to be carried out in order to theoretically understand the physical origin of the strain effect in the electrical conduction of p-type 3C-SiC. Additionally, in this thesis, the experimental approach was utilized to address the magnitude, the orientation dependence, and the temperature dependence of the piezoresistance of p-type 3C-SiC. The experimental data obtained in this work will be significant for the perspective theoretical work on the physical phenomenon of strain effect in p-type 3C-SiC.

2.2 The Piezoresistive Coefficients of 3C-SiC

2.2.1 Definition of the Piezoresistive Coefficients

As mentioned in Chap. 1, the relative resistivity change of a 3C-SiC resistance caused by a mechanical strain can be expressed as a function of the gauge factor (GF) of a semiconductor and the applied strain:

$$\frac{\Delta\rho}{\rho} = GF \times \varepsilon \tag{2.23}$$

In addition, this change of resistivity ($\Delta\rho/\rho$) is connected to the applied stress (σ) through a parameter named piezoresistive coefficient (π):

$$\Delta\rho/\rho = \pi\sigma \tag{2.24}$$

Furthermore, when a uniaxial stress is applied, the relationship between the stress and strain follows Hooke's law: $\sigma = E\varepsilon$, where E is the Young's modulus of SiC. Thus, the relationship between the gauge factor and the piezoresistive coefficient is $GF = E\pi$ [20].

In a general case, where stresses are applied in arbitrary crystallography orientations as shown in Fig. 2.9, the change of resistivity $\Delta\rho_{\mathrm{ij}}$ is a second rank tensor, which is connected to stress tensors (σ_{kl}) by a forth-rank piezoresistive coefficient tensor (π_{ijkl}) [21]:

$$\frac{\Delta\rho_{\mathrm{ij}}}{\rho} = \sum_{\mathrm{k,l}} \pi_{\mathrm{ijkl}}\sigma_{\mathrm{kl}} \tag{2.25}$$

where, i and j denote the directions of the applied current and voltage, while k and l indicate the orientations of the applied stress tensor, respectively. The forth-rank piezoresistive coefficient tensor can be collapsed to a second rank tensor (e.g. $\pi_{1111} \to \pi_{11}, \pi_{1122} \to \pi_{12}$, and $\pi_{2323} \to \pi_{44}$), using the transformation scheme shown in Table 2.1 [20]. Equation 2.25 and Table 2.1 also show that in a three dimensional coordinate, the number of stress components is 6, while the number of piezoresistive coefficients is $6 \times 6 = 36$. However, since 3C-SiC has a symmetric crystalline structure, the number of basic piezoresistive coefficients reduces to 3 in the principal coordinate. The relationship and the applied stress tensors in single crystalline 3C-SiC can be represented in a matrix form as follows:

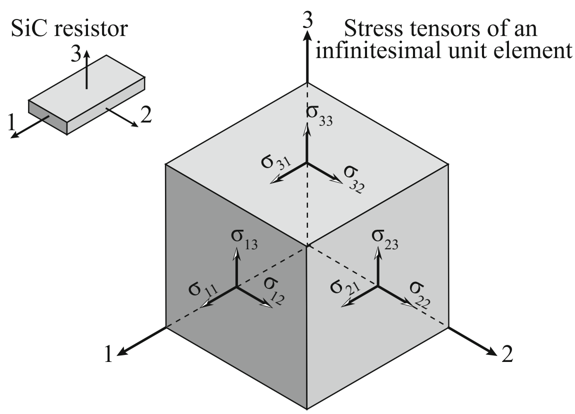

Fig. 2.9 The nine stress components σ_{kl} of an infinitesimal unit element of SiC

Table 2.1 Index transformation scheme

Tensor notation	11	22	33	23 and 32	13 and 31	12 and 21
Matrix notation	1	2	3	4	5	6

$$\begin{pmatrix} \frac{\delta\rho_{11}}{\rho_{11}} \\ \frac{\delta\rho_{22}}{\rho_{22}} \\ \frac{\delta\rho_{33}}{\rho_{33}} \\ \frac{\delta\rho_{23}}{\rho_{23}} \\ \frac{\delta\rho_{13}}{\rho_{13}} \\ \frac{\delta\rho_{12}}{\rho_{12}} \end{pmatrix} = \begin{pmatrix} \pi_{11} & \pi_{12} & \pi_{12} & 0 & 0 & 0 \\ \pi_{12} & \pi_{11} & \pi_{12} & 0 & 0 & 0 \\ \pi_{12} & \pi_{12} & \pi_{11} & 0 & 0 & 0 \\ 0 & 0 & 0 & \pi_{44} & 0 & 0 \\ 0 & 0 & 0 & 0 & \pi_{44} & 0 \\ 0 & 0 & 0 & 0 & 0 & \pi_{44} \end{pmatrix} \begin{pmatrix} \varepsilon_{11} \\ \varepsilon_{22} \\ \varepsilon_{33} \\ \varepsilon_{23} \\ \varepsilon_{13} \\ \varepsilon_{12} \end{pmatrix} \tag{2.26}$$

The fundamental piezoresistive coefficients π_{11}, π_{12}, and π_{44} are very important in defining the orientations dependence of piezoresistive effect, as well as to determine which orientation offers the largest sensitivity for mechanical sensing devices [22].

2.2.2 *Piezoresistive Coefficients of Two-Terminal and Four-Terminal Resistors*

There are two types of piezoresistors which are widely deployed in MEMS sensors [23]. The most common type is the two-terminal resistor where the directions of applied electrical field vector (E) and the current density vector (J) are the same, Fig. 2.10a. The relationship between the change of resistivity and applied stress can be described as follows:

$$\frac{\Delta\rho}{\rho} = \pi'_{11}\sigma_1 + \pi'_{12}\sigma_2 + \pi'_{13}\sigma_3 + \pi'_{14}\sigma_4 + \pi'_{15}\sigma_5 + \pi'_{16}\sigma_6 \tag{2.27}$$

where, σ_1, σ_2, and σ_3 are normal stresses, while σ_4, σ_5, and σ_6 is a shear stress which corresponds. The prime superscription denotes the piezoresistive coefficients in the

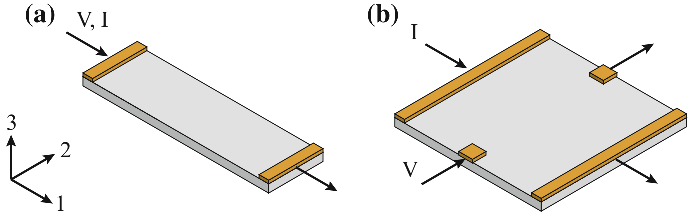

Fig. 2.10 Concept of SiC resistors. **a** Two-terminal resistor; **b** Four-terminal resistor

coordinate of the piezoresistor but not in the principal coordinate. For the case of piezoresistors fabricated using thin films, the piezoresistive coefficient components in the direction perpendicular to applied electric field and current (also known as the out of plane direction) are negligible, because the influence of the stress components in this direction is considered to be insignificant. Therefore, the relative resistance change of thin film resistors under stress is deduced as:

$$\frac{\Delta\rho}{\rho} = \pi'_{11}\sigma_1 + \pi'_{12}\sigma_2 + \pi'_{16}\sigma_6 \tag{2.28}$$

Given that the direction of applied current is the longitudinal orientation, while the direction perpendicular to current is the transverse orientation, Eq. 2.28 can be represented as:

$$\frac{\Delta\rho}{\rho} = \pi_{\mathrm{l}}\sigma_{\mathrm{l}} + \pi_{\mathrm{t}}\sigma_{\mathrm{t}} + \pi_{\mathrm{s}}\sigma_{\mathrm{s}} \tag{2.29}$$

where the subscriptions l, t, and s indicate longitudinal, transverse, and shear components.

The second type of piezoresistors is four-terminal devices [24, 25], Fig. 2.10b. The piezoresistive effect in these devices have attracted considerable attention, since it can be deployed to investigate the influence of stress on the offset voltage in Hall devices. The principle of the piezoresistive effect in two-terminal resistors is that, when a stress is applied to the device, a voltage will be generated at two electrodes which are are aligned in a direction perpendicular to the supplied current. Since this voltage is generated due to strain/stress, without requiring an external magnetic field like the case of Hall devices, the piezoresistive effect in two-terminal resistors is also called the pseudo-Hall effect. Additionally, the ratio between the generated voltage and applied current is defined as a pseudo resistance ρ_{pseudo}, which is connected to the applied stress tensor through the shear piezoresistive coefficients [24, 26]:

$$\frac{V}{I} = \rho_{\mathrm{pseudo}} = \pi'_{61}\sigma_1 + \pi'_{62}\sigma_2 + \pi'_{63}\sigma_6 + \pi'_{64}\sigma_4 + \pi'_{65}\sigma_5 + \pi'_{66}\sigma_6 \tag{2.30}$$

Similar to the case of thin film two-terminal resistors, for thin film four-terminal resistors, the stress components related to the out of plane direction are negligible. Consequently, the generated pseudo resistance can be approximated as:

$$\rho_{\mathrm{pseudo}} = \pi'_{61}\sigma_1 + \pi'_{62}\sigma_2 + \pi'_{66}\sigma_6 \tag{2.31}$$

For both two-terminal and four-terminal devices, the normal piezoresistive coefficients (e.g. π'_{11} and π'_{12}) and shear coefficients (π'_{61} and π'_{62}) can be estimated based on the basic coefficient π_{11}, π_{12} and π_{44}. Therefore, understanding these basic coefficients can represent the piezoresistive coefficients in any crystallographic orientation, and thus can predict which directions offer a large piezoresistive effect. The transformation of piezoresistive coefficient in arbitrary Cartesian coordinate is presented in the following subsection.

2.2.3 *Piezoresistive Coefficients in Arbitrary Cartesian Coordinate*

Given that X, Y, Z are the principal axis, and X', Y', Z' are the coordinate of a piezoresistor, the Cartesian coordinate of the piezoresistor can be obtained from the principal coordinate using the axes transformation illustrated in Fig. 2.11. The first rotation is by an angle ϕ about Z axis; the second rotation is about Y_1 axis an angle of θ; and the third rotation is about Z_2 axis an angle of φ, as illustrated in Fig. 2.11. Additionally, the coordinate x', y', z' in the coordinate of piezoresistor can be transformed from the coordinate x, y, z displayed in the principle Cartesian system, using the following equation:

$$\begin{pmatrix} x' \\ y' \\ z' \end{pmatrix} = \begin{pmatrix} l_1 & m_1 & n_1 \\ l_2 & m_2 & n_2 \\ l_3 & m_3 & n_3 \end{pmatrix} \begin{pmatrix} x \\ y \\ z \end{pmatrix} \tag{2.32}$$

Here $l_{\rm i}$, $m_{\rm j}$, and $n_{\rm k}$ (where, i, j, k $\in \{1, 2, 3\}$) are directional cosine, which are calculated from the rotation angles ϕ, θ, and φ, using the Euler rotation matrix:

$$\begin{pmatrix} l_1 & m_1 & n_1 \\ l_2 & m_2 & n_2 \\ l_3 & m_3 & n_3 \end{pmatrix} = \begin{pmatrix} \cos\phi\cos\theta\cos\varphi - \sin\phi\cos\varphi & \sin\phi\cos\theta\cos\varphi + \cos\phi\sin\varphi & -\sin\phi\cos\varphi \\ -\cos\phi\cos\theta\sin\varphi - \sin\phi\cos\varphi & -\sin\phi\cos\theta\sin\varphi + \cos\phi\cos\varphi & \sin\theta\sin\varphi \\ \cos\phi\sin\theta & \sin\phi\sin\theta & \cos\theta \end{pmatrix} \tag{2.33}$$

Using Euler's rotation theory, the piezoresistive coefficient tensors in the Cartesian system of a piezoresistor can be calculated from the principle piezoresistive coefficient tensor in the principal coordinate, using the following equation [27]:

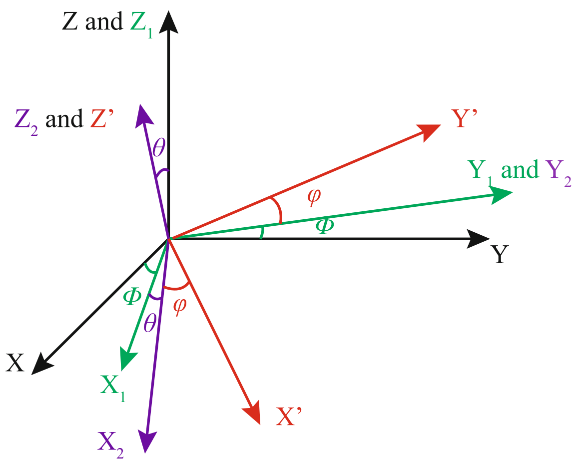

Fig. 2.11 Euler's rotation angles

Table 2.2 Piezoresistive coefficients in arbitrary coordinate

Coeff.	Expressions	Coeff.	Expressions
π'_{11}	$\pi_{11} - 2\pi_C(l_1^2 m_1^2 + m_1^2 n_1^2 + n_1^2 l_1^2)$	π'_{61}	$\pi_C(l_1^3 l_2 + m_1^3 m_2 + n_1^3 n_2)$
π'_{12}	$\pi_{12} + \pi_C(l_1^2 l_2^2 + m_1^2 m_2^2 + n_1^2 n_2^2)$	π'_{62}	$\pi_C(l_1 l_2^3 + m_1 m_2^3 + n_1 n_2^3)$
π'_{13}	$\pi_{12} + \pi_C(l_1^2 l_3^2 + m_1^2 m_3^2 + n_1^2 n_3^2)$	π'_{63}	$\pi_C(l_1 l_2 l_3^2 + m_1 m_2 m_3^2 + n_1 n_2 n_3^2)$
π'_{14}	$2\pi_C(l_1^2 l_2 l_3 + m_1^2 m_2 m_3 + n_1^2 n_2 n_3)$	π'_{64}	$2\pi_C(l_1 l_2^2 l_3 + m_1 m_2^2 m_3 + n_1 n_2^2 n_3)$
π'_{15}	$\pi_C(l_1^3 l_3 + m_1^3 m_3 + n_1^3 n_3)$	π'_{65}	$2\pi_C(l_1^2 l_2 l_3 + m_1^2 m_2 m_3 + n_1^2 n_2 n_3)$
π'_{16}	$2\pi_C(l_1^3 l_2 + m_1^3 m_2 + n_1^3 n_2)$	π'_{66}	$\pi_{44} + 2\pi_C(l_1^2 l_2^2 + m_1^2 m_2^2 + n_1^2 n_2^2)$

$\pi_C \equiv \pi_{11} - \pi_{12} - \pi_{44}$

$$(\pi_{ij}) = \alpha^{-1} \begin{pmatrix} \pi_{11} & \pi_{12} & \pi_{12} & 0 & 0 & 0 \\ \pi_{12} & \pi_{11} & \pi_{12} & 0 & 0 & 0 \\ \pi_{12} & \pi_{12} & \pi_{11} & 0 & 0 & 0 \\ 0 & 0 & 0 & \pi_{44} & 0 & 0 \\ 0 & 0 & 0 & 0 & \pi_{44} & 0 \\ 0 & 0 & 0 & 0 & 0 & \pi_{44} \end{pmatrix} \alpha \tag{2.34}$$

where:

$$\alpha = \begin{pmatrix} l_1^2 & m_1^2 & n_1^2 & 2m_1n_1 & 2n_1l_1 & 2l_1m_1 \\ l_2^2 & m_2^2 & n_2^2 & 2m_2n_2 & 2n_2l_2 & 2l_2m_2 \\ l_3^2 & m_3^2 & n_3^2 & 2m_3n_3 & 2n_3l_3 & 2l_3m_3 \\ l_2l_3 & m_2m_3 & n_2n_3 & m_2n_3 + m_3n_2 & n_2l_3 + n_3l_2 & m_2l_3 + l_3m_2 \\ l_3l_1 & m_3m_1 & b_3n_1 & m_3n_1 + m_1n_3 & n_3l_1 + n_1l_3 & m_3l_1 + l_1m_3 \\ l_1l_2 & m_1m_2 & b_1n_2 & m_1n_2 + m_2n_1 & n_1l_1 + n_2l_1 & m_1l_2 + l_2m_1 \end{pmatrix} \tag{2.35}$$

Based on Eq. 2.35, the transformation of the piezoresistive coefficients of two-terminal and four-terminal resistors in any crystallographic orientation are presented in Table 2.2 [27].

References

1. D. Olego, M. Cardona, P. Vogl, Pressure dependence of the optical phonons and transverse effective charge in 3 C-SiC. Phys. Rev. B **25**(6), 3878 (1982)
2. M. Wijesundara, R. Azevedo, *Silicon Carbide Microsystems for Harsh Environments* (Springer Science & Business Media, Berlin, 2011)
3. G.L. Harris, *Properties of Silicon Carbide*, vol. 13 (IET, London, 1995)
4. S.M. Sze, K.K. Ng, *Physics of Semiconductor Devices* (Wiley, New York, 2006)
5. J.M. Ziman, *Principle of the Theory of Solids* (Cambridge University Press, London, 1964)
6. L.A. Hemstreet Jr., C.Y. Fong, Electronic band structure and optical properties of 3C-SiC, BP, and BN. Phys. Rev. B **6**(4), 1464 (1972)
7. W.P. Eaton, J.H. Smith, Micromachined pressure sensors: review and recent developments. Smar. Mater. Struct. **6**, 530–539 (1997)
8. J.C. Wolfe, Summary of the Kronig–Penney electron. Am. J. Phys. **46**, 1012 (1978)

9. A.C.H. Rowe, Piezoresistance in silicon and its nanostructures. J. Mater. Res. **29**(6), 731–744 (2014)
10. D.L. Pulfrey, *Understanding Modern Transistors and Diodes* (Cambridge University Press, London, 2010)
11. G.L. Bir, G.E. Pikus, in *Symmetry and Strain-Induced Effects in Semiconductors*, vol. 624, ed. by D. Louvish (Wiley, New York, 1974)
12. T. Toriyama, S. Sugiyama, Analysis of piezoresistance in p-type silicon for mechanical sensors. J. Microelectromech. Syst. **11**(5), 598 (2002)
13. P. Kleimann, B. Semmache, M. Le Berre, D. Barbier, Stress-dependent hole effective masses and piezoresistive properties of p-type monocrystalline and polycrystalline silicon. Phys. Rev. B **57**(15), 8966–8971 (1998)
14. Y. Sun, S.E. Thompson, T. Nishida, *Strain Effect in Semiconductor: Theory and Device Applications*, 1st edn. (Springer, Berlin, 2009)
15. H.-P. Phan, D.V. Dao, K. Nakamura, S. Dimitrijev, N.-T. Nguyen, The piezoresistive effect of SiC for MEMS sensors at high temperatures: a review. J. Microelectromech. Syst. **24**(6), 1663–1677 (2015)
16. C. Kong, W. Wang, K. Liao, Y. Ma, S. Wang, L. Fang, The theoretical studies of piezoresistive effect in diamond films. Sci. China Ser. A Math. **45**(1), 107–114 (2002)
17. L. Fang, W.L. Wang, P.D. Ding, K.J. Liao, J. Wang, Study on the piezoresistive effect of crystalline and polycrystalline diamond under uniaxial strains. J. Appl. Phys. **86**, 5185 (1999)
18. W. Lu, K. Zhang, X. Xe, Strain effects on the band structures of β-SiC. Phys. Condens. Matter **5**, 883–890 (1993)
19. R. Rahimi, C.M. Miller, S. Raghavan, C.D. Stinespring, D. Korakakis, Electrical properties of strained nano-thin 3C-SiC/Si heterostructures. J. Phys. D Appl. Phys. **42**, 055108 (2009)
20. A.A. Barlian, W.T. Park, J.R. Mallon Jr., A.J. Rastergar, B.L. Pruit, Review: semiconductor the piezoresistive effect for microsystems. Proc. IEEE **97**(3), 513–552 (2009)
21. Y. Kanda, The piezoresistive effect of silicon. Sens. Actuators A **28**, 83–91 (1991)
22. Y. Kanda, A graphical representation of the piezoresistance coefficients in silicon. IEEE Trans. Electron Devices **29**(1), 64–70 (1982)
23. J.C. Doll, B.L. Pruitt, *Piezoresistor Design and Applications* (Springer, Berlin, 2013). ISBN 978-1-4614-8516-2
24. Y. Kanda, K. Yamamura, Four terminal gauge quasi circular and square diaphragm silicon pressure sensors. Sens. Actuators **19**, 247–257 (1989)
25. A. Mian, J.C. Suhling, R.C. Jaeger, The van der Pauw Stress Sensor. IEEE Sens. J. **6**(2), (2006)
26. D.V. Dao, T. Toriyama, J. Wells, S. Sugiyama, Silicon piezoresistive six-degree of freedom micro force-moment sensor. Sens. Mater. **15**, 113–135 (2002)
27. M.H. Bao, *Micro Mechanical Transducers: Pressure Sensors, Accelerometers and Gyroscopes*, vol. 8 (Elsevier, Amsterdam, 2000)

Springer

http://www.springer.com/978-3-319-55543-0

Piezoresistive Effect of p-Type Single Crystalline 3C-SiC
Silicon Carbide Mechanical Sensors for Harsh
Environments
Phan, H.-P.
2017, XXI, 146 p. 94 illus., 3 illus. in color., Hardcover
ISBN: 978-3-319-55543-0